Journal of Medicinal Chemistry

pubs.acs.org/jmc

Drug Annotation

Discovery of AZD4831, a Mechanism-Based Irreversible Inhibitor of Myeloperoxidase, As a Potential Treatment for Heart Failure with Preserved Ejection Fraction

Tord Inghardt,* Thomas Antonsson, Cecilia Ericsson, Daniel Hovdal, Petra Johannesson, Carina Johansson, Ulrik Jurva,* Johan Kajanus, Bengt Kull, Erik Michaëlsson, Anna Pettersen, Tove Sjögren, Henrik Sörensen, Kristina Westerlund, and Eva-Lotte Lindstedt

Cite This: *J. Med. Chem.* 2022, 65, 11485−11496

Read Online

ACCESS | Metrics & More | Article Recommendations | Supporting Information

ABSTRACT: Myeloperoxidase is a promising therapeutic target for treatment of patients suffering from heart failure with preserved ejection fraction (HFpEF). We aimed to discover a covalent myeloperoxidase inhibitor with high selectivity for myeloperoxidase over thyroid peroxidase, limited penetration of the blood−brain barrier, and pharmacokinetics suitable for once-daily oral administration at low dose. Structure−activity relationship, biophysical, and structural studies led to prioritization of four compounds for in-depth safety and pharmacokinetic studies in animal models. One compound (AZD4831) progressed to clinical studies on grounds of high potency (IC_{50}, 1.5 nM *in vitro*) and selectivity (>450-fold *vs* thyroid peroxidase *in vitro*), the mechanism of irreversible inhibition, and the safety profile. Following phase 1 studies in healthy volunteers and a phase 2a study in patients with HFpEF, a phase 2*b*/3 efficacy study of AZD4831 in patients with HFpEF started in 2021.

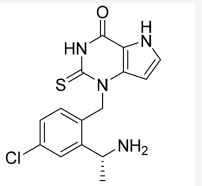

AZD4831 (MPO IC_{50}=2nM)

INTRODUCTION

Heart failure is a systemic syndrome in which the metabolic demands of the organs are not met by the cardiac output and has a prevalence as high as 10% among people aged over 60 years.[1] Nearly half of patients with chronic heart failure have heart failure and a preserved ejection fraction (HFpEF; left ventricular ejection fraction ≥50%), and the 5-year mortality of patients with HFpEF is estimated to be 30%. Coronary microvascular dysfunction is highly prevalent and correlates with disease severity, systemic endothelial dysfunction, and diastolic dysfunction in patients with HFpEF.[2,3] Treatment options are limited for patients with HFpEF, and a novel pharmacological intervention that improve macro- and microvascular structure and function would be beneficial.

Myeloperoxidase (MPO) is a microbicidal heme-containing enzyme of the innate immune system that is produced by neutrophils in the bone marrow and stored in their lysosomal azurophilic granules, with some production also by monocytes and macrophages. Upon activation, neutrophils release MPO into the phagolysosomal compartment where it catalyzes the reaction of hydrogen peroxide with halides to form reactive oxygen intermediates such as hypochlorous acid. Some MPO is also released extracellularly following neutrophil degranulation, resulting in generation of oxidizing species that can cause tissue damage.[4−6]

MPO has been implicated in the pathogenesis of several inflammatory conditions, including HFpEF,[7] coronary artery disease,[4,8] chronic kidney disease,[4,9] chronic obstructive pulmonary disease,[10] nonalcoholic steatohepatitis,[11,12] and rheumatoid arthritis.[4,13] Plasma MPO levels independently predict risks of myocardial infarction and other major cardiac events,[14] and the enzyme is localized to atherosclerotic plaques and implicated in atherogenesis.[15] Elevated MPO levels are associated with more advanced heart failure and correlate with microvascular dysfunction.[16,17] MPO is therefore a promising therapeutic target in HFpEF and other cardiovascular diseases.[6] MPO is closely related to eosinophil peroxidase (EPO) and exocrine gland-expressed lactoperoxidase (LPO), for which the associations with disease are less clear. Another peroxidase, thyroid peroxidase (TPO), is expressed in the thyroid gland, where its iodination activity is required for the generation of thyroid hormone T_4 (thyroxine). TPO plays an important role in endocrine function and therefore represents a peroxidase toward which a therapeutic margin is desired.[6]

On a molecular level, native-state (ferric) MPO is activated by hydrogen peroxide, which is formed within the cells via the dismutation of the superoxide anion produced by NADPH oxidase (Figure 1). This two-electron oxidation forms an active MPO-ferryl cation π radical known as "compound I". Compound I is a highly reactive species that can react with halides (Cl^-, Br^-, and I^-) and pseudohalides (SCN^-) to form

Received: December 15, 2021
Published: August 25, 2022

https://doi.org/10.1021/acs.jmedchem.1c02141
J. Med. Chem. 2022, 65, 11485−11496

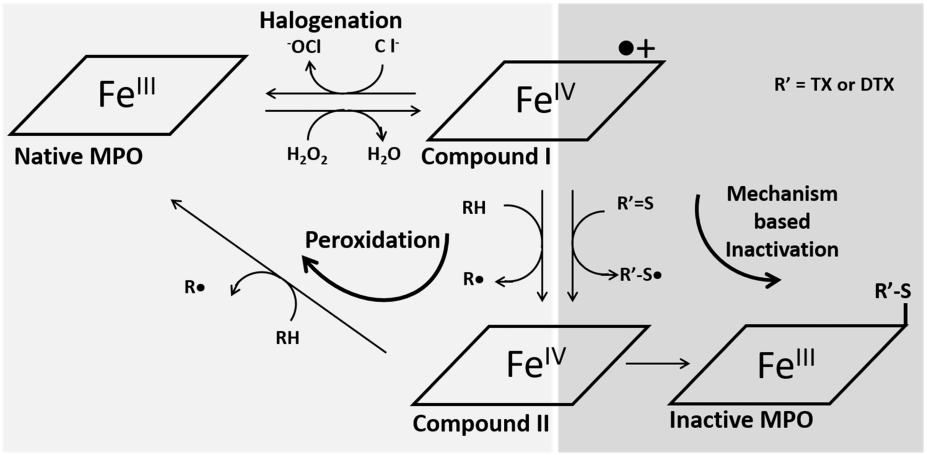

Figure 1. Enzymatic cycles of myeloperoxidase. MPO is activated by hydrogen peroxide and is converted into the highly reactive species "compound I", through a two-electron oxidation. "Compound I" can react with halides (Cl^-, Br^-, I^-) and pseudohalides (SCN^-) to form the corresponding hypohalous acid and reduce MPO back to the native state. This is known as the halogenation cycle.[18] "Compound I" can also act as a peroxidase by sequentially reacting with single-electron donors to form the redox intermediate "compound II", which is in turn reduced back to the native state. This is known as the peroxidase cycle. Thioxanthines (TX) or deazathioxanthines (DTX) can react with "compound I" to form an inactive species of MPO.[20,21]

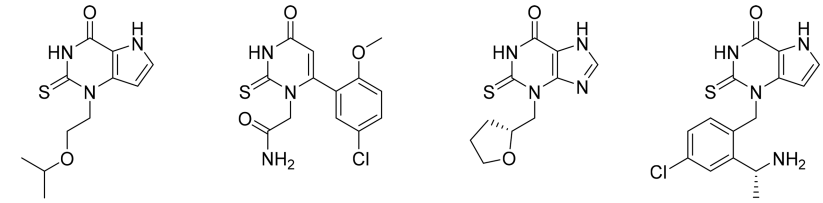

1 (Verdiperstat, BHV-3241/AZD3241)

2 (Pfizer, PF-06282999 WO2013/068875 (Ex1))

3 (AZD5904)

16 (AZD4831)

Figure 2. Myeloperoxidase inhibitors evaluated in clinical trials.

the corresponding hypohalous acid and reduce MPO back to the native state. This is known as the halogenation cycle.[18] Compound I can also act as a peroxidase by sequentially reacting with single-electron donors to form the redox intermediate compound II, which is in turn reduced back to the native state. This is known as the peroxidase cycle.[18] A variety of reversible inhibitors, in the form of single-electron donors that thereby compete with the halogenation cycle for compound I, have been described.[19] Compound II can, however, easily be reduced back to the native state by endogenous substrates, such as serotonin, urate, ascorbate, or tyrosine, and re-enter the catalytic cycle. Selective irreversible inactivation of the active forms to inhibit both halogenation and peroxidation may be an effective strategy to inhibit MPO. We and others have previously reported that 2-thioxanthines ("R′ = S") are mechanism-based, covalent inhibitors ("suicide substrates") of MPO.[20,21] In a single-electron reaction (Figure 1), a highly reactive thiyl radical ("R′-S•") is formed by compound I and reacts rapidly *in situ* with one of the methyl groups of the heme in compound II. This forms a covalent complex and irreversibly inactivates the enzyme, avoiding production and release of potentially harmful radicals.[20]

Several mechanism-based irreversible inhibitors of MPO have progressed to clinical trials (*e.g.* compounds **1**, **2**, **3**, and **16**, Figure 2). Verdiperstat (**1**; previously BHV-3241 and AZD3241) is currently being evaluated for treatment of multiple system atrophy in a phase 3 study (NCT03952806) and for treatment of amyotrophic lateral sclerosis (ALS) as part of the HEALEY ALS platform study (NTC04436510). Development of the Pfizer compound PF-06282999 (**2**)[22] was terminated in phase 1, possibly due to drug−drug interaction concerns.[23,24] AZD5904 (**3**) has been evaluated in phase 1 studies and is available within the AstraZeneca open innovation initiative. Here, we report the discovery of the potent, selective, and irreversible MPO inhibitor AZD4831 (**16**), which is in clinical trials for treatment of patients with HFpEF.

RESULTS

***In Vitro* Pharmacology and Structure−Activity Relationship Studies.** We aimed to identify a low-dose, once-daily oral MPO inhibitor with high selectivity for MPO over TPO and limited penetration of the blood−brain barrier. As a starting point for new MPO inhibitors, the aliphatic side chains of compounds **1** and **3** were replaced with benzylic groups (as in **4**),[20] leading to improved potency but with only a minor improvement in selectivity over TPO (Table 1).

In screening and structure−activity relationship mapping of our candidate MPO inhibitors, we measured IC_{50} against purified MPO and TPO in an *in vitro* chemiluminescent assay (Table 1; Supporting Information). Exploration of phenyl substituents revealed that a strongly basic secondary amine in an ortho (2-) phenyl side chain was well tolerated and conferred 10-fold greater selectivity for MPO than TPO (**5** vs

https://doi.org/10.1021/acs.jmedchem.1c02141
J. Med. Chem. 2022, 65, 11485−11496

Table 1. Structure, Potency, Selectivity, and Irreversibility of MPO Inhibitors[a]

Compound	Structure	MPO IC_{50} (nM)	TPO IC_{50} (μM)	MPO/TPO selectivity ratio	HL60 cell IC_{50} (μM)	Irreversibility (fold EC_{50} shift)
2	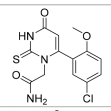	187.0	0.99	5	35.5	1.91
3	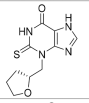	279.1	2.40	9	29.0	1.36
4	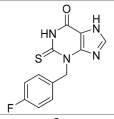	32.0	0.59	18	No data	1.57
5	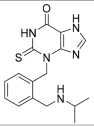	38.6	4.20	109	80.0	0.87
6	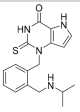	30.9	8.10	262	13.0	1.01
7	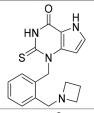	15.1	1.50	99	6.6	1.13
8	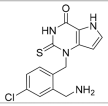	15.0	1.30	87	11.0	0.78
9	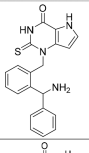	5.0	1.39	278	No data	1.06
10	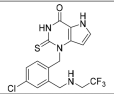	35.0	3.40	97	1.3	1.40
11	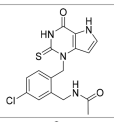	140.3	1.40	10	16.0	1.12
12	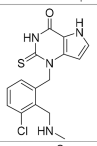	39.3	4.20	107	9.4	0.84
13	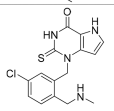	27.1	1.90	70	6.1	0.81
14	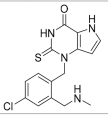	15.9	2.10	132	6.6	1.16
15*	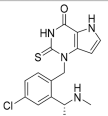	12.7	1.10	87	4.6	0.72
16	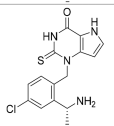	1.5	0.69	460	0.8	0.80
17	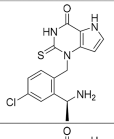	26.4	1.10	42	20.0	1.31
18	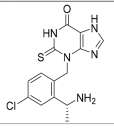	3.6	0.77	214	3.1	1.03

[a]MPO, myeloperoxidase; TPO, thyroid peroxidase. HL60 is a human promyelocytic leukemia cell line. *Compound **15** is a pure enantiomer but the absolute stereochemistry has not been determined.

4; Table 1). The selectivity for MPO over TPO was further improved when the thioxanthine scaffold was replaced by deaza thioxanthine (DTX; **5** vs **6**). Introduction of a tertiary amine into the phenyl side chain (**7**) slightly improved potency compared with compound **6**, but selectivity for MPO over TPO was reduced. Selectivity for MPO over TPO was further reduced when a primary amine was introduced (**8**). Adding a benzylic phenyl group to the primary amine (**9**) improved potency and selectivity for MPO over TPO (>250 fold) compared with all our previous compounds. Reduction of amine basicity (**10**) was tolerated with modest loss of MPO activity compared with compound **9**, but acylation of the amine (**11**) resulted in major loss of potency as well as selectivity for MPO versus TPO.

Chlorination at phenyl positions 3- (**12**), 4- (**14**), and 5- (**13**) was well tolerated, with position 4- yielding the highest potency and selectivity for MPO. Methylation of the benzylic position next to the thioxanthine/DTX ring system led to a major drop in potency (data not shown), but a methyl group introduced at the benzyl carbon next to the amine (**15**) resulted in potency and selectivity for MPO over TPO similar to that of compound **14**. Returning to a primary amine (**16**) dramatically improved MPO potency and selectivity compared with compound **15**. The *R* enantiomer (**16**) was clearly superior to the *S* enantiomer (**17**), with 10-fold higher MPO potency and selectivity. When the DTX scaffold of compound **16** was replaced with thioxanthine (**18**), selectivity for MPO over TPO was reduced more than 2-fold.

In a cell-based assay (HL60 promyelocytic leukemia cells differentiated into neutrophil-like cells), we observed an average drop-off of 500-fold (range, 40- to 2000-fold) in the potency of our MPO inhibitors, compared with purified enzyme assays. This may be related to the high intragranular concentration of MPO, estimated to be in the millimolar range.[25] The observed difference in potency agrees with published data on intragranular *vs* extracellular MPO inhibition in primary human neutrophils.[26] The lower potency for intragranular MPO inhibition suggests that our inhibitors may have limited effects on the microbicidal function of MPO.

To assess irreversibility of inhibition, we developed a tight binding assay as an alternative to the "partition ratio" (rapid dilution) assay reported by others (Table 1).[22] We measured activity of purified MPO immobilized to anti-MPO-coated ELISA plates, before and after repeated washing to remove the

https://doi.org/10.1021/acs.jmedchem.1c02141
J. Med. Chem. 2022, 65, 11485−11496

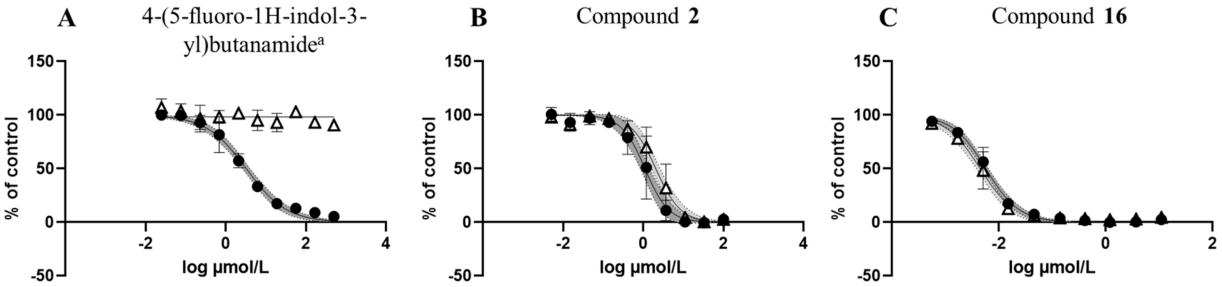

Figure 3. Tight binding assay with human myeloperoxidase and inhibitors. Concentration−response curves obtained with (A) the reversible inhibitor 4-(5-fluoro-1H-indol-3-yl)butanamide; (B) compound 2, indicating partial reversibility; and (C) compound 16, indicating irreversible inhibition. ● represents inhibition in the presence of the inhibitor (before washing) and the △ represents inhibition without re-addition of inhibitor after repeated washing. Shaded areas represent 95% confidence intervals for the modeled inhibition. Data are mean and standard deviation of results from triplicate wells.

inhibitor. With the reversible inhibitor 4-(5-fluoro-1H-indol-3-yl)butanamide, inhibition was lost upon washing and reactivation (Figure 3A).[27] Compound **2** has been described as a partially reversible inhibitor (partition ratio 6.5),[22] but it maintained most of the inhibitory activity upon reactivation after washing, with a 1.91-fold shift in EC_{50} (Figure 3B; Table 1). In contrast, our MPO inhibitors exhibited even greater irreversibility of binding, with shifts in EC_{50} for compounds **5**, **8**, **12**, **13**, **15**, and **16** ranging from 0.72 to 0.87 (Figure 3C; Table 1). We also evaluated the potency of compound **16** on the structurally related EPO and noted an approximately 50-fold drop in potency compared with MPO. Inhibition of EPO was irreversible as judged by the persistent inhibition in a corresponding EPO tight binding assay.

BIOPHYSICAL AND STRUCTURAL CHEMISTRY

To guide design of our MPO inhibitor compounds, we sought to understand the structure of the initial ligand−MPO recognition complex. Addition of thioxanthines to the highly reactive compound I state (Figure 1) would immediately result in enzyme turnover and covalent product formation. Therefore, as a surrogate, we studied binding of our compounds to native-state MPO without addition of hydrogen peroxide, using a 1D NMR reporter assay. These native-state structures could not provide a complete picture of binding events, so they were only used for reference rather than classical structure-based design. IC_{50} values for our MPO inhibitors with native MPO were considerably higher than with compound I, but the hierarchy was maintained with a strong linear correlation (r^2 = 0.96) (Table 2).

The structures of the MPO inhibitors **3** and **9** bound to native MPO were determined to 2.1 Å. The thioxanthine moiety of compound **3** binds at the entrance of the narrow distal heme cavity and is oriented such that the thioxanthine plane is nearly coplanar with the D pyrrole ring of the heme, with the carbonyl oxygen pointing toward the solvent atom coordinated to the heme iron (Figure 4A). The thioxanthine core is engaged in hydrogen bonds with the heme carboxylate group and the side chain of Arg 239. The electron density for the aliphatic side chain extends into the globular cavity adjacent to the narrow heme pocket, but the electron density is weak, indicating flexibility. In contrast, compound **9** has a 100-fold higher NMR dissociation constant (K_d) and a well resolved side chain (Figure 4B). The side chain occupies an entirely different part of the adjacent cavity, with the primary amine hydrogen-bonded to solvent molecules. Notably, neither of the compounds make any significant interactions with the protein. If the native-state binding mode is indeed a surrogate of the compound I recognition complex, the inhibitor would need to reorient to form the irreversible complex, where the thioxanthine moiety is oriented perpendicular to the heme D pyrrole ring.[20] The side chain would need to be accommodated in both binding modes. These complex binding events could account for the diversity in potency, partition ratio, and selectivity for MPO versus TPO in the series, despite conservation of the thioxanthine core.

Table 2. Native-State MPO Equilibrium Dissociation Constants[a]

compound	pK_d NMR[b] (n = 1)	pIC_{50} MPO (n = 3)
3	4.2	6.6
4	4.7	7.5
8	5.4	7.8
9	6.2	8.9
16	6.3	8.8

[a] K_d, dissociation constant; MPO, myeloperoxidase; and NMR, nuclear magnetic resonance. [b] Determined by competition experiments with benzohydroxamic acid (pK_d = 2.3).[20]

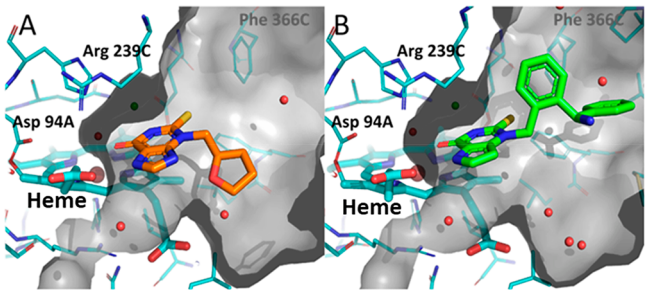

Figure 4. Native myeloperoxidase in complex with (A) compound **3** and (B) compound **9**. Myeloperoxidase is shown in blue stick representation and compounds **3** and **9** are shown in orange and green, respectively. The coordinates have been deposited in the PDB with coordinates 7NI1 and 7NI3.

Physical Chemistry and *in Vitro* Drug Metabolism and Pharmacokinetics. Physicochemical properties and selected *in vitro* drug metabolism and pharmacokinetic properties are shown in Table 3 for compounds **5**−**18**.

Most of the MPO inhibitors (all except **9**, **10**, and **11**) occupied a favorable physicochemical space, with a log D between 0.5 and 1.5 and solubility between 18 μM and 930

https://doi.org/10.1021/acs.jmedchem.1c02141
J. Med. Chem. 2022, 65, 11485−11496

Table 3. Physicochemical and *in Vitro* Drug Metabolism and Pharmacokinetic Properties of Compounds 5−18[a]

compound number	log *D*	solubility at pH 7.4 (μM)	human liver microsome intrinsic clearance (μL/min/mg)	rat hepatocyte intrinsic clearance (μL/min/10^6 cells)	human hepatocyte intrinsic clearance (μL/min/10^6 cells)	caco-2 cell intrinsic permeability (10^6 cm/s)[b]	early dose to human prediction (mg/day)[c]
5	0.3	18	<3	<1	<1	0.89	150
6	0.9	140	4.5	11	<1	12	110
7	1.0	930	<3	19	<1	19	71
8	1.2	42	<3	3.2	3.2	6.0	180
9	1.7	8.3[b]	39	20	1.9	18	14
10	3.3	0.37	8.2	30	4.3	49	1000
11	2.0	3.3	<3	<1	<1	11	630
12	1.3	150	11	15	<1	19	290
13	1.1	210	3.3	21	<1	9.6	120
14	1.3	160	<3	2.4	<1	17	68
15	1.5	190	5.5	5.6	<1	19	49
16	1.2	270	<3	1.8	<1	11	8
17	1.4	850	<3	<1	<1	10	97
18	0.7	880	<3	<1	<1	1.3	15

[a]Unless otherwise indicated, values are the mean of three replicates. [b]n = 2. [c]Early dose to human predictions were based on a composite of myeloperoxidase (MPO) IC_{50} and metabolic stability in human hepatocytes. A free steady state plasma level of 10 times MPO IC_{50} was assumed as a requirement for functional efficacy *in vivo* (see the Supporting Information).

Table 4. Safety and Pharmacokinetic Parameters of Compounds 8, 14, 16, and 18[a]

compound number	hERG channel IC_{50} (μM) (n = 3)	CYP3A4 IC_{50} (μM) (n = 3)	rat clearance (mL/min/kg) (n = 2)	rat *F* (%) (n = 2)	dog clearance (mL/min/kg) (n = 2)	dog *F* (%) (n = 2)
8	>40	19	32[b]	68	19	45
14	10	>30	22	60	23	72
16	21	6.0	19[b]	61	5.7	52
18	23	8.8	20	7.4	no data	no data

[a]CYP3A4, cytochrome P450 3A4; F, bioavailability; hERG, human ether-à-go-go-related gene (potassium voltage-gated channel subfamily H member 2 isoform a). [b]n = 4.

μM. They generally also had high metabolic stability in human liver microsomes and rat and human hepatocytes, as well as high intrinsic Caco-2 cell permeability. Compounds with decreased pK_a of the amine moiety displayed reduced solubility compared with the other compounds, exemplified by the CF_3 ethyl compound **10** and the N-acetylated compound **11**. DTX compounds generally had higher permeability than thioxanthine compounds (illustrated by the DTX/thioxanthine matched pairs **6**/**5** and **16**/**18**), which we attribute to the increased lipophilicity and decreased polar surface area of the DTX compounds compared with thioxanthine compounds. Increased lipophilicity of compound **11** was accompanied by decreased metabolic stability.

To aid rapid prioritization of compounds, we used an "early dose to human" prediction based on a composite of MPO IC_{50} and metabolic stability in human hepatocytes (Table 3; Supporting Information).

Safety Profile and *in Vivo* Pharmacokinetics of Selected MPO Inhibitors. On the basis of overall assessment of the early dose to human predictions and other properties shown in Table 3, compounds **8**, **14**, **16**, and **18** were selected for extensive profiling, including safety parameters and pharmacokinetics in rats and dogs (Table 4).

Compounds **14**, **16**, and **18** were moderate inhibitors of the potassium ion channel encoded by human ether-à-go-go-related gene (hERG), and compounds **8**, **16**, and **18** were weak competitive inhibitors of cytochrome P450 (CYP) 3A4, with no time-dependent inhibition. No inhibition of other CYP isoforms (2D6, 2C9, 1A2, and 2C19) was detected (IC_{50} > 30 μM). Given predicted plasma exposures to free drug of around 100 nM, we deemed the safety margin for hERG and CYP inhibition to be acceptable for all four compounds.

Compounds **8**, **14**, and **16** displayed moderate clearance and high oral bioavailability in rats. Conversely, the thioxanthine compound (**18**) had a very low oral bioavailability, likely due to low intrinsic permeability as demonstrated in Caco-2 cell screens, and was not progressed to dog PK studies. The remaining three compounds had good oral bioavailability in dogs. Compound **16** was substantially more stable than compounds **8** and **14**, with a clearance of 5.7 mL/min/kg compared with 19 mL/min/kg and 23 mL/min/kg, respectively. In a separate experiment in rats, the unbound central nervous system exposure of compound **16** was determined to be 0.7% of the unbound exposure in plasma, indicating limited penetration of the blood-brain barrier. Given the mechanism-based, covalent mechanism of action, we performed several studies with compounds **8** and **16** to assess the potential for nonspecific covalent binding.

Mechanism of Nonspecific Covalent Binding. The results of covalent binding experiments with ^{14}C-labeled compound **8** and AZD4831 (**16**) revealed moderate covalent binding in human hepatocytes (95 and 56 pmol/mg protein, respectively). Further experiments were conducted with [^{14}C]-**8** in human liver microsomes to better understand the binding mechanism. Incubations with and without NADPH gave similar levels of covalent binding, suggesting that the mechanism is not mediated by CYPs (Figure 5). Heat inactivation of the microsomes did not affect covalent binding (Figure 5), which led to the hypothesis that the mechanism was nonenzymatic and originated from a chemical reaction

https://doi.org/10.1021/acs.jmedchem.1c02141
J. Med. Chem. 2022, 65, 11485−11496

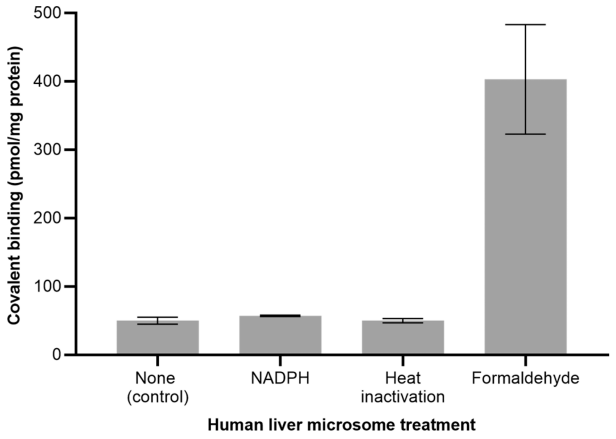

Figure 5. Covalent binding of compound [^{14}C]-8 in human liver microsomes.

between the parent drug and constituents of the proteins. A chemical reactivity study with KCN added as a trapping reagent for unstable intermediates gave a cyanomethylene amine product. A plausible mechanism for the formation of this product (**Q**) via an initial reaction with formaldehyde is given in Scheme 1.

The nonenzymatic covalent binding (CVB) is hypothesized to originate from reaction of the imine intermediate with hepatic proteins.

The presence of formaldehyde was attributed to impurity in the ethanol used in the assay. Published *in vivo* levels of formaldehyde are between 0.1 and 0.4 mM,[28] so it is reasonable to assume that sufficient levels are present in human hepatocytes to facilitate the moderate levels of covalent binding observed. Addition of 5 mM formaldehyde to the human liver microsome incubations led to a substantial increase in covalent binding (Figure 5), demonstrating that formaldehyde can mediate the chemical reaction. We hypothesize that the imine intermediate in Scheme 1 is the main mechanism of covalent binding, although others cannot be excluded.

Risk Assessment for Nonspecific Covalent Binding. An exploratory, quantitative whole-body autoradiography study in rats, including extraction of tissue slices, was performed to assess the risk of nonspecific covalent binding of AZD4831 (**16**) to tissue *in vivo*. Chemical reactivity is not expected to vary between species, making this a good safety model. The nonextractable fraction in the liver 24 h after an oral dose of 10 MBq/kg of [^{14}C]-**16** was less than 0.2% (Figure 6). Radioactivity was retained in pigmented skin and in the eyes for longer than in other tissues, which was expected because basic compounds commonly bind noncovalently to melanin.[29] After 7 days, only 0.1% of drug-related material was detected in the whole body. On the basis of these results, the risk of nonenzymatic covalent tissue binding of AZD4831 (**16**) was judged to be low.

On the basis of the above results, AZD4831 (**16**) was selected as a potential clinical candidate and progressed into extended safety and toxicology testing. Assessment of the potential cardiovascular effect was performed both *in vitro* and *in vivo* to follow up potential signals from the optimization phase, e.g., hERG channel IC_{50} (Table 4). This work included an *in vitro* ion channel panel and *in vivo* evaluation of cardiac effects in anesthetized guinea pigs and cardiac telemetry in dogs. Furthermore, AZD4831 was not genotoxic in the Ames test, the mouse lymphoma assay, or the rat bone marrow micronucleus assay and was not phototoxic in the Balb/c 3T3 cell neutral red uptake assay. For long-term *in vivo* toxicology studies, the rat and the dog were selected as model species because they were considered to be pharmacologically relevant and because the major human metabolites had been detected in rat and/or dog plasma. At the time of writing, AZD4831 (**16**) has been evaluated in pivotal toxicological studies for up to 6 months in rats and 9 months in dogs (Supporting Information). In the 6-month rat study, dose levels up to 125 mg/kg/day were generally well tolerated, and the "no observed adverse effect level" (NOAEL) was therefore considered to be 125 mg/kg/day in both males and females. In the 9-month dog study, dose levels up to 100 mg/kg/day were well tolerated with no effects on food consumption, body weight, or pathology, and NOAEL was therefore considered to be 100 mg/kg/day.

In summary, a sufficient preclinical safety profile and margin to predicted therapeutic exposure was established and AZD4831 (**16**) progressed to clinical studies. Currently, a phase 2*b*/3 clinical study in patients with HFpEF is ongoing with a once-daily oral dose range of 2.5 to 5 mg (ENDAVOUR; NCT04986202).

***In vivo* Pharmacology of AZD4831.** The efficacy of AZD4831 (**16**) was evaluated in BALB/c mice with zymosan-induced neutrophilic peritonitis. Compound **16** (10, 1, 0.1, and 0.01 μmol/kg) was administered orally 2 h before zymosan injection, and MPO activity in peritoneal lavage was quantified 2 h later by chemiluminescent assay. The AZD4831 dose dependently inhibited the peroxidase activity in lavage fluid (Figure 7). Because neutrophils dominate the cellular infiltrate at this time point in the zymosan model, this activity was assumed to result from MPO rather than other peroxidases. Systemic drug exposure was dose-dependent, with a mean total

Scheme 1. Tentative Mechanism for Formation of the Cyanomethylene Amine (Q) from Compound 8

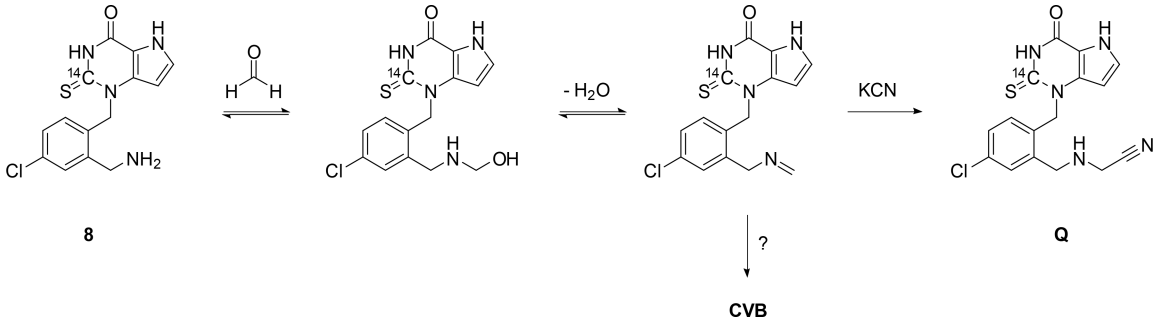

https://doi.org/10.1021/acs.jmedchem.1c02141
J. Med. Chem. 2022, 65, 11485−11496

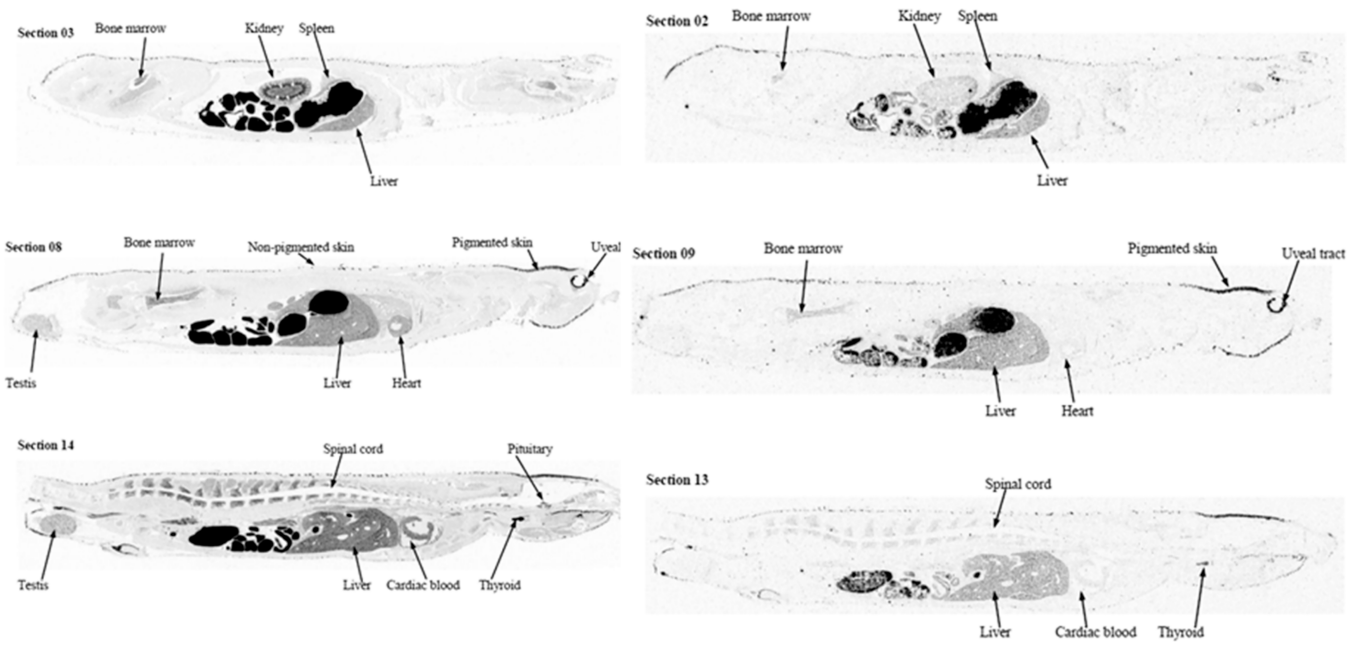

Figure 6. Whole-body autoradiography 24 h after an oral dose of [^{14}C]-16 (AZD4831) in rats, before (left) and after (right) extraction.

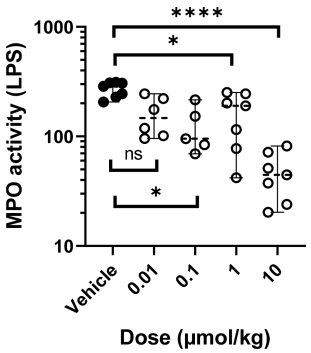

Figure 7. Dose-dependent inhibition of peritoneal myeloperoxidase by compound **16** (AZD4831) in mice. ****$p < 0.0001$. *$p < 0.05$; ns, not significant. Data are expressed as photons per second (LPS), and each symbol represents one mouse. The statistical analysis was performed on log-transformed data by one-way analysis of variance followed by Dunnett's multiple comparison test.

plasma concentration of 1.7 nM at 4 h after a minimally effective dose of 0.1 μmol/kg. The potency of AZD4831 is approximately five times lower for mouse than human MPO (unpublished data), so these estimates agree with the potency observed for extracellular MPO, rather than for intragranular MPO in HL60 cells and primary neutrophils (Table 1).

We have also investigated the impact of MPO inhibition in disease and mechanistic models in collaboration with academic partners. These studies demonstrated efficacy of compound **8** (also referred to in the literature as "AZM198") in ameliorating vascular function,[30] atherosclerotic plaque biology,[31] pulmonary hypertension,[32] renal disease,[33] visceral inflammatory fat deposition, ectopic fat deposition, and hepatic fibrosis.[1134] These processes are all potential culprits in the complex pathophysiology of HFpEF.

Predicting Clinical Pharmacology from Preclinical Data. On the basis of the associations between MPO deficiency, heparin-mediated release of vascular MPO and vascular function in humans,[17,35] and between vascular function and clinical outcomes,[36] 50% inhibition of MPO activity was postulated to be clinically meaningful. The relevance of this estimate is also supported by the effect size of the decreased MPO activity associated with the AA/AG versus AA genotypes of the −463 *MPO* promoter that has been reported to confer protection against coronary artery disease and heart failure.[37−39]

At the point of candidate drug nomination, we adopted a more conservative dose prediction based on a generic assumption that 80% inhibition would be needed for efficacy, using *in vitro* binding kinetics and inactivation rate constants derived for the drug−MPO complex in the chemiluminescence assay. We simulated the concentration−time profile of AZD4831 (**16**) in humans using a one-compartment model (Figure 8).[40] On the basis of enzyme kinetics and pharmacokinetic modeling, a once-daily dose of 20 mg was predicted to generate a total plasma drug concentration of 31 nM and unbound plasma drug concentrations of 11 nM at the end of each dosing interval (see the Supporting Information).

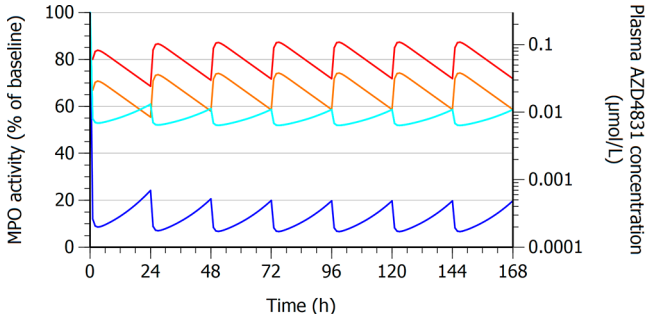

Figure 8. Predicted myeloperoxidase activity and plasma drug concentration versus time after once-daily oral dosing of 20 mg of compound **16** (AZD4831) in humans. Dark blue line shows the total inhibition of myeloperoxidase activity relative to the baseline, and the light blue line shows the contribution from irreversible inhibition. Red and orange lines show the predicted total and unbound plasma concentration of compound **16**, respectively.

https://doi.org/10.1021/acs.jmedchem.1c02141
J. Med. Chem. 2022, 65, 11485−11496

Scheme 2. Synthesis of Compound 16 (AZD4831)[a]

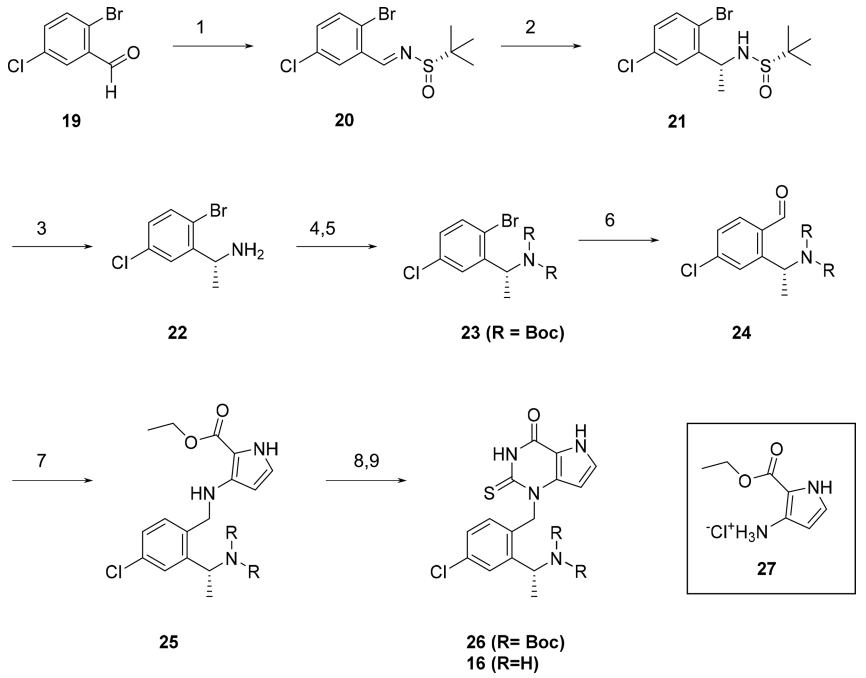

[a](1) (*S*)-2-methylpropane-2-sulfinamide, Cs_2CO_3, and DCM, reflux. (2) MeMgBr and DCM, −45 °C to rt. (3) HCl and MeOH. (4) Boc_2O, TEA, and DCM. (5) Boc_2O, DMAP, and 2-MeTHF. (6) CO:H_2 (1:1, 5 bar), $Pd(OAc)_2$, cataCXium A, TMEDA, and toluene, 100 °C. (7) (i) **27**, DIPEA, EtOH, (ii) HOAc, and (iii) $NaBH_3CN$. (8) (i) Benzoylsothiocyanate, MeOH, rt and (ii) C_2CO_3, 60 °C. (9) HCl and MeOH, 50 °C.

We recently reported results from two phase 1 studies of AZD4831 (**16**) in healthy volunteers, one using single ascending doses[41] and one using multiple ascending dosing to steady state.[42] Results indicated that exposure in humans was well predicted from the preclinical pharmacokinetic data. Full human absorption, distribution, metabolism, and excretion data from a recently completed phase 1 clinical trial of [^{14}C]-AZD4831 (NCT04407091) will be published elsewhere. After a single dose of 15 mg AZD4831,[41] maximal plasma concentration (C_{max}) and concentration at 24 h (C_{24h}) were accurately predicted (observed vs expected C_{max}, 83.4 nM vs 81.8 nM; observed vs expected C_{24h}, 20 nM vs 18.2 nM), and the area under the concentration−time curve from time zero to infinity ($AUC_{0-\infty}$) was slightly underpredicted (observed vs predicted $AUC_{0-\infty}$ of 1669 nmol h/L vs 1193 nmol h/L). The likely reason for the underprediction of AUC was that we used a model with a monoexponential decline of the drug concentration, while the observed concentration−time profiles showed a biexponential decline with a longer terminal half-life ($t_{1/2}$) than predicted ($t_{1/2,obs}$ ∼45 h vs $t_{1/2,pred}$ ∼ 11 h), mainly due to a larger volume of distribution than predicted. The consequence of this flatter pharmacokinetic profile was that the targeted unbound trough concentration after multiple doses (11 nM) was obtained in the low end of the predicted dose range: 5 mg in healthy volunteers and 2.5 mg in patients with HFpEF.[42]

Synthetic Chemistry. The synthesis of AZD4831 (**16**) is described in Scheme 2 (see the Supporting Information for abbreviations and synthesis and characterization of other compounds). The synthesis of the chiral amine **22** relied upon the chemistry developed by Ellman et al.[43] and commenced with condensation of aldehyde **19** and (*S*)-2-methylpropane-2-sulfinamide to the corresponding (*S*)-sulfinylimine **20. 20** was subjected to a highly diastereoselective 1,2-addition of methylmagnesium bromide to give enantiomerically pure **21** after chromatographic separation from the minor diastereomer. The stereochemical outcome in the 1,2-addition of the Grignard reagent agrees with the transition state model proposed by Ellman and co-workers[44] for noncoordinating solvents and was also confirmed by vibrational circular dichroism (VCD) spectroscopy (Supporting Information). Treatment of **21** with HCl/MeOH gave amine **22** which was subjected to a two-step *N-di*-Boc protection to form compound **23.** This protection was necessary to avoid an intramolecular cyclization reaction with the aldehyde function introduced in the upcoming step. The aldehyde **24** was synthesized from the bromide **23** by a palladium-catalyzed formylation reaction with $Pd(OAc)_2$/cataCXium A as precatalyst, tetramethylethylenediamine as base, and synthesis gas as the formyl source as described by Beller and co-workers.[45]

Reductive amination of aldehyde **24** with amine hydrochloride **27** using $NaBH_3CN$ as the reducing agent gave amine **25.** Reaction of amine **25** with bensoyl isothiocyanate followed by direct addition of Cs_2CO_3 to the reaction mixture gave the cyclized product **26**. Finally, deprotection of the two Boc groups in **26** with HCl/MeOH gave enantiomerically pure (*R*) **16** (*ee* = 99.9%). The absolute stereochemistry of **16** was determined by single crystal X-ray crystallography of a mesylate salt (Supporting Information).

SUMMARY AND CONCLUSIONS

AZD4831 (**16**) is a novel covalent MPO inhibitor with high selectivity for MPO over TPO at low oral doses. We designed, synthesized, and preclinically evaluated a series of MPO inhibitors that bind covalently to compound II in the peroxidation cycle of MPO. AZD4831 (**16**) was identified as a candidate for further clinical development because of its high

https://doi.org/10.1021/acs.jmedchem.1c02141
J. Med. Chem. 2022, 65, 11485−11496

in vitro potency, selectivity for MPO over TPO, and mechanism of irreversible MPO inhibition. Preclinical efficacy assessments in animal models showed that AZD4831 dose-dependently inhibits MPO, and safety assessments did not reveal any findings of concern. In phase 1 clinical studies in healthy volunteers, AZD4831 was generally well tolerated, was rapidly absorbed with a long plasma half-life, and dose-dependently inhibited MPO in whole blood.[41,42] In a phase 2a clinical study of AZD4831 (**16**) in patients with HFpEF, target engagement (inhibition of MPO) was confirmed and in exercise capacity (6 min walking distance) and health-related quality of life (Kansas City Cardiomyopathy Questionnaire—overall summary score) increased numerically (SATELLITE; NCT03756285; manuscript in preparation). A phase 2*b*/3 dose-finding and efficacy study in patients with HFpEF started in July 2021 (ENDEAVOR; NCT04986202).

EXPERIMENTAL SECTION

Purity. All screening compounds had purity greater than 95% (see the Supporting Information).

*(S)-N-[(2-Bromo-5-chloro-phenyl)methylene]-2-methylpropane-2-sulfinamide (**20**).* 2-Bromo-5-chlorobenzaldehyde (4.00 g, 18.2 mmol) was dissolved in DCM (130 mL), and (*S*)-2-methylpropane-2-sulfinamide (2.32 g, 19.1 mmol) was added followed by Cs_2CO_3 (5.94 g, 18.2 mmol). The reaction mixture was refluxed overnight and then diluted with brine and DCM. The organic layer was filtered through a phase separator and concentrated *in vacuo*. The crude product was purified by automated flash chromatography using a gradient of 0–25% EtOAc in heptane to yield **20** (5.60 g, 95%) as a solid. ^{1}H NMR (400 MHz, $(CD_3)_2SO$): δ 8.75 (s, 1H), 7.98 (d, J = 2.7 Hz, 1H), 7.84 (d, J = 8.6 Hz, 1H), 7.61 (dd, J = 8.6, 2.7 Hz, 1H), 1.21 (s, 9H).

*(S)-N-[(1R)-1-(2-Bromo-5-chloro-phenyl)ethyl]-2-methylpropane-2-sulfinamide (**21**).* Compound **20** (5.41 g, 16.8 mmol) was dissolved in DCM (200 mL) under a nitrogen atmosphere and cooled to −45 °C. Methylmagnesium bromide (3 M in diethyl ether, 11.2 mL, 33.6 mmol) was added dropwise at −45 °C. The reaction mixture was stirred at between −40 and −50 °C for 4 h and then allowed to reach rt overnight. A saturated aqueous solution of NH_4Cl (50 mL) was added followed by water (100 mL). The layers were separated using a phase separator, and the aqueous layer was extracted with DCM (3 × 150 mL). The combined organic layers were concentrated *in vacuo*. The residue was purified by automated flash chromatography using a gradient of 10–60% EtOAc in heptane to yield **21** (5.28 g, 93%). The absolute configuration of the title compound was determined by VCD spectroscopy. ^{1}H NMR (400 MHz, $(CD_3)_2SO$): δ 7.57–7.64 (m, 2H), 7.27 (dd, J = 8.5, 2.6 Hz, 1H), 5.63 (d, J = 5.9 Hz, 1H), 4.70 (p, J = 6.6 Hz, 1H), 1.44 (d, J = 6.7 Hz, 3H), 1.11 (s, 9H).

*(1R)-1-(2-Bromo-5-chloro-phenyl)ethanamine Hydrochloride (**22**).* Sulfinamide **21** (5.25 g, 15.5 mmol) was treated with a methanol solution of HCl (1.25 M; 150 mL, 187.5 mmol) at rt for 1.5 h. The solvent was removed *in vacuo*. The remainder was dissolved in DCM (200 mL) and washed with a saturated aqueous solution of $NaHCO_3$ (100 mL). The aqueous layer was extracted with DCM (200 mL), and the combined organic layers were concentrated *in vacuo* to give the hydrogen chloride salt of **22** (4.02 g, quantitative yield) which was used in the next step without further purification. ^{1}H NMR (400 MHz, $CDCl_3$): δ 7.55 (d, *J* = 2.6 Hz, 1H), 7.44 (d, *J* = 8.5 Hz, 1H), 7.07 (dd, *J* = 8.4, 2.6 Hz, 1H), 4.46 (q, *J* = 6.6 Hz, 1H), 1.36 (d, *J* = 6.5 Hz, 3H).

*tert-Butyl N-[(1R)-1-(2-Bromo-5-chloro-phenyl)ethyl]-N-tert-butoxycarbonyl-carbamate (**23**).* Triethylamine (2.6 mL, 18.6 mmol) and Boc_2O (3.73 g, 17.1 mmol) were added to a solution of **22** (3.64 g, 15.5 mmol) in DCM (150 mL). The reaction mixture was stirred at rt for 3.5 h and then washed with 1 M aqueous solution of potassium bisulfate (100 mL). The aqueous phase was extracted with DCM (100 mL), and the combined organic layers were concentrated *in vacuo* to give mono-Boc protected intermediate *tert*-butyl N-[(1R)-1-(2-bromo-5-chloro-phenyl)ethyl]carbamate (5.83 g, quantitative yield). ^{1}H NMR (400 MHz, $CDCl_3$): δ 7.45 (d, *J* = 8.5 Hz, 1H), 7.31 (s, 1H), 7.08 (dd, *J* = 8.5, 2.5 Hz, 1H), 4.98 (d, *J* = 34.0 Hz, 2H), 1.3–1.5 (m, 12H).

Tert-butyl [(1*R*)-1-(2-bromo-5-chlorophenyl)ethyl]carbamate (5.19 g, 15.5 mmol) was dissolved in 2-MeTHF (150 mL), and Boc_2O (5.08 g, 23.3 mmol) and DMAP (2.84 g, 23.3 mmol) were added. The reaction mixture was stirred at rt for 16 h, whereupon more Boc_2O (1.69 g, 7.8 mmol) and DMAP (0.95 g, 7.8 mmol) were added. The mixture was stirred at 50 °C for 4.5 h and then concentrated *in vacuo*. The residue was redissolved in DCM (150 mL) and washed with 1 M aqueous solution of $KHSO_4$ (100 mL). The aqueous phase was extracted with DCM (100 mL), and the combined organic layers were concentrated *in vacuo*. The residue was purified twice by automated flash chromatography using a gradient of 0–20% EtOAc in heptane to yield **23** (5.05 g, 75%). ^{1}H NMR (400 MHz, $(CD_3)_2SO$): δ 7.64 (d, *J* = 8.4 Hz, 1H), 7.55 (d, *J* = 2.6 Hz, 1H), 7.33 (dd, *J* = 8.5, 2.6 Hz, 1H), 5.33 (q, *J* = 7.0 Hz, 1H), 1.55 (d, *J* = 7.0 Hz, 3H), 1.36 (s, 18H).

*tert-Butyl N-tert-Butoxycarbonyl-N-[(1R)-1-(5-chloro-2-formyl-phenyl)ethyl]carbamate (**24**).* Bromide **23** (4.27 g, 9.83 mmol), $Pd(OAc)_2$ (0.221 g, 0.98 mmol), cataCXium A (1.06 g, 2.95 mmol), and tetramethylethylenediamine (1.1 mL, 7.4 mmol) were dissolved in toluene (18 mL), and the reaction mixture was sealed in an autoclave. The autoclave was filled with synthesis gas ($CO:H_2$, 1:1) at 5 bar and then heated in an oil-bath for 21 h at 100 °C. The crude product was purified by automated flash chromatography using a gradient of 0–20% EtOAc in heptane to yield aldehyde **24** (2.15 g, 57%). ^{1}H NMR (400 MHz, $(CD_3)_2SO$): δ 10.14 (s, 1H), 7.87 (d, *J* = 8.3 Hz, 1H), 7.67 (d, *J* = 2.1 Hz, 1H), 7.61 (dd, *J* = 8.2, 2.1 Hz, 1H), 6.06 (q, *J* = 6.9 Hz, 1H), 1.58 (d, *J* = 6.9 Hz, 3H), 1.34 (s, 18H).

*Ethyl 3-[[2-[(1R)-1-[bis(tert-Butoxycarbonyl)amino]ethyl]-4-chloro-phenyl]methylamino]-1H-pyrrole-2-carboxylate (**25**).* To a mixture of ethyl 3-amino-1*H*-pyrrole-2-carboxylate hydrochloride (1.14 g, 5.99 mmol) and EtOH (99.5%, 20 mL) was added diethylamine (1.8 mL, 10 mmol), followed by **24** (2.00 g, 5.21 mmol) dissolved in EtOH (99.5%, 5 mL). The reaction mixture was stirred at rt overnight. HOAc (0.90 mL, 16 mmol) was added, and the mixture was stirred at rt for 6 h. $NaBH_3CN$ (0.344 g, 5.47 mmol) was added portion-wise over a period of 3 min, and the reaction mixture was stirred at rt for 1 h, diluted with water, and extracted with a mixture of EtOAc (25 mL) and toluene (25 mL). The aqueous phase was extracted with additional EtOAc (25 mL). The combined organic layers were washed twice with an aqueous solution of citric acid (0.5 M; 25 mL), twice with an aqueous solution of $NaHCO_3$, and with brine. The solution was dried over $MgSO_4$, and the solvent was removed *in vacuo* to give **25** (2.93 g, quantitative yield). ^{1}H NMR (400 MHz, $(CD_3)_2SO$): δ 10.78 (s, 1H), 7.42 (s, 1H), 7.28–7.35 (m, 2H), 6.69 (t, *J* = 3.2 Hz, 1H), 5.81 (s, 1H), 5.51 (q, *J* = 6.8 Hz, 1H), 5.42 (t, *J* = 2.6 Hz, 1H), 4.36 (dd, *J* = 16.4, 6.2 Hz, 1H), 4.14–4.26 (m, 3H), 1.59 (d, *J* = 6.8 Hz, 3H), 1.31 (s, 18H). LC–MS (ESI) *m*/*z*: 522.8 (calculated for $C_{26}H_{36}ClN_3O_6$ $[M + H]^+$, 522.2).

*tert-Butyl N-tert-Butoxycarbonyl-N-[(1R)-1-[5-chloro-2-[(4-oxo-2-thioxo-5H-pyrrolo[3,2-d]pyrimidin-1-yl)methyl]phenyl]ethyl]-carbamate (**26**).* Benzoyl isothiocyanate (0.647 mL, 4.81 mmol) was added dropwise to a solution of **25** (2.79 g, 4.01 mmol) dissolved in MeOH (12 mL), and the resulting mixture was stirred at rt overnight followed by addition of cesium carbonate (2.74 g, 8.42 mmol). The mixture was heated at 60 °C for 3 h and then cooled to 10 °C. HOAc (1.0 mL, 18 mmol) was added slowly followed by a slow addition of water (24 mL). The formed precipitate was collected by filtration and washed with MeOH to give **26** (1.835g, 85%) as a beige solid. Used as such in the next step. LC–MS (ESI) *m*/*z*: 533.7 (calculated for $C_{25}H_{31}ClN_4O_5S$ $[M - H]^-$, 533.2).

*(R)-1-(2-(1-Aminoethyl)-4-chlorobenzyl)-2-thioxo-2,3-dihydro-1H-pyrrolo[3,2-d]pyrimidin-4(5H)-one (**16**).* Compound **26** (0.933 g, 1.74 mmol) was treated with HCl in methanol (1.25 M) (24 mL, 30 mmol). The reaction mixture was stirred at 50 °C for 1 h and then cooled in an ice-bath. Water (3 mL) was added, followed by a slow addition of an aqueous solution of ammonia (25%) to pH 9.3. The

https://doi.org/10.1021/acs.jmedchem.1c02141
J. Med. Chem. 2022, 65, 11485–11496

formed precipitate was collected by filtration to obtain compound **16** (0.388 g, 67%) as a beige solid with an enantiomeric excess of 99.9%. [α]D20 = +76.8° (c = 0.3, MeOH). ^{1}H NMR (400 MHz, $(CD_3)_2SO$): δ 7.65 (d, J = 2.3 Hz, 1H), 7.31 (d, J = 2.8 Hz, 1H), 7.11 (dd, J = 8.3, 2.4 Hz, 1H), 6.59 (d, J = 8.4 Hz, 1H), 6.04 (d, J = 2.8 Hz, 1H), 5.58−5.87 (m, 2H), 4.36 (q, J = 6.5 Hz, 1H), 1.32 (d, J = 6.5 Hz, 3H). 13C NMR (151 MHz, $(CD_3)_2SO$) δ 173.5, 152.6, 148.2, 136.9, 131.8, 130.8, 128.1, 126.3, 126.1, 125.5, 113.7, 96.9, 49.9, 46.1, 24.6. HRMS (ESI) m/z: 335.0710 (calculated for C15H15ClN4OS [M + H]$^+$, 335.0733).

■ ASSOCIATED CONTENT

Supporting Information

The Supporting Information is available free of charge at https://pubs.acs.org/doi/10.1021/acs.jmedchem.1c02141.

Synthesis procedures, drug metabolism and pharmacokinetic assays, tables with data including statistics; NMR spectra, vibrational circular dichroism spectra, and enantiomeric excess; and HPLC traces (PDF)

SMILES codes and selected data for compounds **1**−**18** Compounds expected and found masses (CSV)

Accession Codes

Authors will release the atomic coordinates upon article publication.

■ AUTHOR INFORMATION

Corresponding Authors

Tord Inghardt − *Research and Early Development, Cardiovascular, Renal and Metabolism, BioPharmaceuticals R&D, AstraZeneca, 431 50 Gothenburg, Sweden;* orcid.org/0000-0002-4804-9474; Email: tord.inghardt@astrazeneca.com

Ulrik Jurva − *Research and Early Development, Cardiovascular, Renal and Metabolism, BioPharmaceuticals R&D, AstraZeneca, 431 50 Gothenburg, Sweden;* Email: ulrik.jurva@astrazeneca.com

Authors

Thomas Antonsson − *Research and Early Development, Cardiovascular, Renal and Metabolism, BioPharmaceuticals R&D, AstraZeneca, 431 50 Gothenburg, Sweden*

Cecilia Ericsson − *Research and Early Development, Cardiovascular, Renal and Metabolism, BioPharmaceuticals R&D, AstraZeneca, 431 50 Gothenburg, Sweden*

Daniel Hovdal − *Research and Early Development, Cardiovascular, Renal and Metabolism, BioPharmaceuticals R&D, AstraZeneca, 431 50 Gothenburg, Sweden*

Petra Johannesson − *Research and Early Development, Cardiovascular, Renal and Metabolism, BioPharmaceuticals R&D, AstraZeneca, 431 50 Gothenburg, Sweden*

Carina Johansson − *Discovery Sciences, BioPharmaceuticals R&D, AstraZeneca, 431 50 Gothenburg, Sweden*

Johan Kajanus − *Research and Early Development, Cardiovascular, Renal and Metabolism, BioPharmaceuticals R&D, AstraZeneca, 431 50 Gothenburg, Sweden*

Bengt Kull − *Research and Early Development, Cardiovascular, Renal and Metabolism, BioPharmaceuticals R&D, AstraZeneca, 431 50 Gothenburg, Sweden*

Erik Michaëlsson − *Research and Early Development, Cardiovascular, Renal and Metabolism, BioPharmaceuticals R&D, AstraZeneca, 431 50 Gothenburg, Sweden*

Anna Pettersen − *Pharmaceutical Sciences, BioPharmaceuticals R&D, AstraZeneca, 431 50 Gothenburg, Sweden;* orcid.org/0000-0002-0025-7936

Tove Sjögren − *Discovery Sciences, BioPharmaceuticals R&D, AstraZeneca, 431 50 Gothenburg, Sweden;* orcid.org/0000-0002-6703-4200

Henrik Sörensen − *Research and Early Development, Cardiovascular, Renal and Metabolism, BioPharmaceuticals R&D, AstraZeneca, 431 50 Gothenburg, Sweden*

Kristina Westerlund − *Research and Early Development, Cardiovascular, Renal and Metabolism, BioPharmaceuticals R&D, AstraZeneca, 431 50 Gothenburg, Sweden*

Eva-Lotte Lindstedt − *Research and Early Development, Cardiovascular, Renal and Metabolism, BioPharmaceuticals R&D, AstraZeneca, 431 50 Gothenburg, Sweden*

Complete contact information is available at: https://pubs.acs.org/10.1021/acs.jmedchem.1c02141

Author Contributions

Conceptualization: T.I., D.H., U.J., E.-L.L., and E.M. Design and synthesis: T.I., T.A., C.E., P.J., U.J., J.K., E.-L.L., H.S., and K.W. Biological evaluation: E.M., B.K., C.J., and D.H. Crystallography: A.P. and T.S. The manuscript was written through contributions of all authors. All authors approved the final version of the manuscript.

Funding

This work was funded by AstraZeneca.

Notes

The authors declare the following competing financial interest(s): All authors are employees of AstraZeneca and own stock or stock options.

■ ACKNOWLEDGMENTS

We thank our AstraZeneca colleagues Terese Andersson, Johan Sundell, and Nicholas Tomkinson for synthesis support and Richard J. Lewis for providing VCD analyses.

■ ABBREVIATIONS USED

Ac, acetyl; ALS, amyotrophic lateral sclerosis; aq, aqueous; AUC, area under the concentration−time curve; CYP, cytochrome P450; DCM, dichloromethane; DMAP, 4-(*N*,*N*-dimethylamino)pyridine; DTX, deaza thioxanthine; EC_{50}, half maximal effective concentration; ELISA, enzyme-linked immunosorbent assay; Et, ethyl; hERG, human ether-à-go-go-related gene; HFpEF, heart failure with preserved ejection fraction; HRMS, high -resolution mass spectrometry; IC_{50}, half-maximum inhibitory concentration; K_d, dissociation constant; LC−MS, liquid chromatography−mass spectrometry; log D, distribution coefficient; Me, methyl; MPO, myeloperoxidase; NADPH, reduced nicotinamide adenine dinucleotide phosphate; NMR, nuclear magnetic resonance; PK, pharmacokinetic; pK_a, inverse log of the acid dissociation constant; rt, room temperature; $t_{1/2}$, terminal half-life; TPO, thyroid peroxidase; VCD, vibrational circular dichroism

■ REFERENCES

(1) van Riet, E. E.; Hoes, A. W.; Wagenaar, K. P.; Limburg, A.; Landman, M. A.; Rutten, F. H. Epidemiology of heart failure: the prevalence of heart failure and ventricular dysfunction in older adults over time. A systematic review. *Eur. J. Heart Fail* **2016**, *18* (3), 242−252.

(2) Hage, C.; Michaelsson, E.; Kull, B.; Miliotis, T.; Svedlund, S.; Linde, C.; Donal, E.; Daubert, J. C.; Gan, L. M.; Lund, L. H. Myeloperoxidase and related biomarkers are suggestive footprints of endothelial microvascular inflammation in HFpEF patients. *ESC Heart Fail* **2020**, *7* (4), 1534−1546.
(3) Shah, S. J.; Lam, C. S. P.; Svedlund, S.; Saraste, A.; Hage, C.; Tan, R. S.; Beussink-Nelson, L.; Ljung Faxen, U.; Fermer, M. L.; Broberg, M. A.; Gan, L. M.; Lund, L. H. Prevalence and correlates of coronary microvascular dysfunction in heart failure with preserved ejection fraction: PROMIS-HFpEF. *Eur. Heart J.* **2018**, *39* (37), 3439−3450.
(4) Aratani, Y. Myeloperoxidase: its role for host defense, inflammation, and neutrophil function. *Arch. Biochem. Biophys.* **2018**, *640*, 47−52.
(5) Davies, M. J.; Hawkins, C. L. The role of myeloperoxidase in biomolecule modification, chronic inflammation, and disease. *Antioxid Redox Signal* **2020**, *32* (13), 957−981.
(6) Davies, M. J. Myeloperoxidase: mechanisms, reactions and inhibition as a therapeutic strategy in inflammatory diseases. *Pharmacol Ther* **2021**, *218*, 107685.
(7) Tromp, J.; Khan, M. A.; Klip, I. T.; Meyer, S.; de Boer, R. A.; Jaarsma, T.; Hillege, H.; van Veldhuisen, D. J.; van der Meer, P.; Voors, A. A. Biomarker profiles in heart failure patients with preserved and reduced ejection fraction. *J. Am. Heart Assoc* **2017**, *6* (4), No. e003989, DOI: 10.1161/JAHA.116.003989.
(8) Nicholls, S. J.; Hazen, S. L. Myeloperoxidase and cardiovascular disease. *Arterioscler Thromb Vasc Biol.* **2005**, *25* (6), 1102−1111.
(9) Correa, S.; Pena-Esparragoza, J. K.; Scovner, K. M.; Waikar, S. S.; Mc Causland, F. R. Myeloperoxidase and the risk of CKD progression, cardiovascular disease, and death in the chronic renal insufficiency cohort (CRIC) study. *Am. J. Kidney Dis* **2020**, *76* (1), 32−41.
(10) Zhu, A.; Ge, D.; Zhang, J.; Teng, Y.; Yuan, C.; Huang, M.; Adcock, I. M.; Barnes, P. J.; Yao, X. Sputum myeloperoxidase in chronic obstructive pulmonary disease. *Eur. J. Med. Res.* **2014**, *19*, 12.
(11) Piek, A.; Koonen, D. P. Y.; Schouten, E. M.; Lindtstedt, E. L.; Michaelsson, E.; de Boer, R. A.; Sillje, H. H. W. Pharmacological myeloperoxidase (MPO) inhibition in an obese/hypertensive mouse model attenuates obesity and liver damage, but not cardiac remodeling. *Sci. Rep* **2019**, *9* (1), 18765.
(12) Pulli, B.; Ali, M.; Iwamoto, Y.; Zeller, M. W.; Schob, S.; Linnoila, J. J.; Chen, J. W. Myeloperoxidase-hepatocyte-stellate cell cross talk promotes hepatocyte injury and fibrosis in experimental nonalcoholic steatohepatitis. *Antioxid Redox Signal* **2015**, *23* (16), 1255−1269.
(13) Wang, W.; Jian, Z.; Guo, J.; Ning, X. Increased levels of serum myeloperoxidase in patients with active rheumatoid arthritis. *Life Sci.* **2014**, *117* (1), 19−23.
(14) Brennan, M. L.; Penn, M. S.; Van Lente, F.; Nambi, V.; Shishehbor, M. H.; Aviles, R. J.; Goormastic, M.; Pepoy, M. L.; McErlean, E. S.; Topol, E. J.; Nissen, S. E.; Hazen, S. L. Prognostic value of myeloperoxidase in patients with chest pain. *N Engl J. Med.* **2003**, *349* (17), 1595−1604.
(15) Daugherty, A.; Dunn, J. L.; Rateri, D. L.; Heinecke, J. W. Myeloperoxidase, a catalyst for lipoprotein oxidation, is expressed in human atherosclerotic lesions. *J. Clin Invest* **1994**, *94* (1), 437−444.
(16) Rudolph, V.; Andrie, R. P.; Rudolph, T. K.; Friedrichs, K.; Klinke, A.; Hirsch-Hoffmann, B.; Schwoerer, A. P.; Lau, D.; Fu, X.; Klingel, K.; Sydow, K.; Didie, M.; Seniuk, A.; von Leitner, E. C.; Szoecs, K.; Schrickel, J. W.; Treede, H.; Wenzel, U.; Lewalter, T.; Nickenig, G.; Zimmermann, W. H.; Meinertz, T.; Boger, R. H.; Reichenspurner, H.; Freeman, B. A.; Eschenhagen, T.; Ehmke, H.; Hazen, S. L.; Willems, S.; Baldus, S. Myeloperoxidase acts as a profibrotic mediator of atrial fibrillation. *Nat. Med.* **2010**, *16* (4), 470−474.
(17) Rudolph, T. K.; Wipper, S.; Reiter, B.; Rudolph, V.; Coym, A.; Detter, C.; Lau, D.; Klinke, A.; Friedrichs, K.; Rau, T.; Pekarova, M.; Russ, D.; Knoll, K.; Kolk, M.; Schroeder, B.; Wegscheider, K.; Andresen, H.; Schwedhelm, E.; Boeger, R.; Ehmke, H.; Baldus, S. Myeloperoxidase deficiency preserves vasomotor function in humans. *Eur. Heart J.* **2012**, *33* (13), 1625−1634.
(18) Davies, M. J. Myeloperoxidase-derived oxidation: mechanisms of biological damage and its prevention. *J. Clin Biochem Nutr* **2010**, *48* (1), 8−19.
(19) Galijasevic, S. The development of myeloperoxidase inhibitors. *Bioorg. Med. Chem. Lett.* **2019**, *29* (1), 1−7.
(20) Tiden, A. K.; Sjogren, T.; Svensson, M.; Bernlind, A.; Senthilmohan, R.; Auchere, F.; Norman, H.; Markgren, P. O.; Gustavsson, S.; Schmidt, S.; Lundquist, S.; Forbes, L. V.; Magon, N. J.; Paton, L. N.; Jameson, G. N.; Eriksson, H.; Kettle, A. J. 2-thioxanthines are mechanism-based inactivators of myeloperoxidase that block oxidative stress during inflammation. *J. Biol. Chem.* **2011**, *286* (43), 37578−37589.
(21) Geoghegan, K. F.; Varghese, A. H.; Feng, X.; Bessire, A. J.; Conboy, J. J.; Ruggeri, R. B.; Ahn, K.; Spath, S. N.; Filippov, S. V.; Conrad, S. J.; Carpino, P. A.; Guimaraes, C. R. W.; Vajdos, F. F. Deconstruction of activity-dependent covalent modification of heme in human neutrophil myeloperoxidase by multistage mass spectrometry (MS(4)). *Biochemistry* **2012**, *51* (10), 2065−2077.
(22) Ruggeri, R. B.; Buckbinder, L.; Bagley, S. W.; Carpino, P. A.; Conn, E. L.; Dowling, M. S.; Fernando, D. P.; Jiao, W.; Kung, D. W.; Orr, S. T.; Qi, Y.; Rocke, B. N.; Smith, A.; Warmus, J. S.; Zhang, Y.; Bowles, D.; Widlicka, D. W.; Eng, H.; Ryder, T.; Sharma, R.; Wolford, A.; Okerberg, C.; Walters, K.; Maurer, T. S.; Zhang, Y.; Bonin, P. D.; Spath, S. N.; Xing, G.; Hepworth, D.; Ahn, K.; Kalgutkar, A. S. Discovery of 2-(6-(5-Chloro-2-methoxyphenyl)-4-oxo-2-thioxo-3,4-dihydropyrimidin-1(2H)-yl)acet amide (PF-06282999): A highly selective mechanism-based myeloperoxidase inhibitor for the treatment of cardiovascular diseases. *J. Med. Chem.* **2015**, *58* (21), 8513−8528.
(23) Dong, J. Q.; Gosset, J. R.; Fahmi, O. A.; Lin, Z.; Chabot, J. R.; Terra, S. G.; Le, V.; Chidsey, K.; Nouri, P.; Kim, A.; Buckbinder, L.; Kalgutkar, A. S. Examination of the human cytochrome P4503A4 induction potential of PF-06282999, an irreversible myeloperoxidase inactivator: integration of preclinical, in silico, and biomarker methodologies in the prediction of the clinical outcome. *Drug Metab. Dispos.* **2017**, *45* (5), 501−511. *Another Pfizer compound, PF-06667272 (structure not published), has been evaluated in a Ph1 trial but was terminated for unknown reasons.*
(24) Moscovitz, J. E.; Lin, Z.; Johnson, N.; Tu, M.; Goosen, T. C.; Weng, Y.; Kalgutkar, A. S. Induction of human cytochrome P450 3A4 by the irreversible myeloperoxidase inactivator PF-06282999 is mediated by the pregnane X receptor. *Xenobiotica* **2018**, *48* (7), 647−655.
(25) Reeves, E. P.; Lu, H.; Jacobs, H. L.; Messina, C. G.; Bolsover, S.; Gabella, G.; Potma, E. O.; Warley, A.; Roes, J.; Segal, A. W. Killing activity of neutrophils is mediated through activation of proteases by K+ flux. *Nature* **2002**, *416* (6878), 291−297.
(26) Bjornsdottir, H.; Welin, A.; Michaelsson, E.; Osla, V.; Berg, S.; Christenson, K.; Sundqvist, M.; Dahlgren, C.; Karlsson, A.; Bylund, J. Neutrophil NET formation is regulated from the inside by myeloperoxidase-processed reactive oxygen species. *Free Radic Biol. Med.* **2015**, *89*, 1024−1035.
(27) Soubhye, J.; Aldib, I.; Elfving, B.; Gelbcke, M.; Furtmuller, P. G.; Podrecca, M.; Conotte, R.; Colet, J. M.; Rousseau, A.; Reye, F.; Sarakbi, A.; Vanhaeverbeek, M.; Kauffmann, J. M.; Obinger, C.; Neve, J.; Prevost, M.; Zouaoui Boudjeltia, K.; Dufrasne, F.; Van Antwerpen, P. Design, synthesis, and structure-activity relationship studies of novel 3-alkylindole derivatives as selective and highly potent myeloperoxidase inhibitors. *J. Med. Chem.* **2013**, *56* (10), 3943−3958.
(28) Tulpule, K.; Dringen, R. Formaldehyde in brain: an overlooked player in neurodegeneration? *J. Neurochem* **2013**, *127* (1), 7−21.
(29) Rimpela, A. K.; Reinisalo, M.; Hellinen, L.; Grazhdankin, E.; Kidron, H.; Urtti, A.; Del Amo, E. M. Implications of melanin binding in ocular drug delivery. *Adv. Drug Deliv Rev.* **2018**, *126*, 23−43.
(30) Cheng, D.; Talib, J.; Stanley, C. P.; Rashid, I.; Michaelsson, E.; Lindstedt, E. L.; Croft, K. D.; Kettle, A. J.; Maghzal, G. J.; Stocker, R. Inhibition of MPO (myeloperoxidase) attenuates endothelial

dysfunction in mouse models of vascular inflammation and atherosclerosis. *Arterioscler Thromb Vasc Biol.* **2019**, *39* (7), 1448−1457.
(31) Rashid, I.; Maghzal, G. J.; Chen, Y. C.; Cheng, D.; Talib, J.; Newington, D.; Ren, M.; Vajandar, S. K.; Searle, A.; Maluenda, A.; Lindstedt, E. L.; Jabbour, A.; Kettle, A. J.; Bongers, A.; Power, C.; Michaelsson, E.; Peter, K.; Stocker, R. Myeloperoxidase is a potential molecular imaging and therapeutic target for the identification and stabilization of high-risk atherosclerotic plaque. *Eur. Heart J.* **2018**, *39* (35), 3301−3310.
(32) Klinke, A.; Berghausen, E.; Friedrichs, K.; Molz, S.; Lau, D.; Remane, L.; Berlin, M.; Kaltwasser, C.; Adam, M.; Mehrkens, D.; Mollenhauer, M.; Manchanda, K.; Ravekes, T.; Heresi, G. A.; Aytekin, M.; Dweik, R. A.; Hennigs, J. K.; Kubala, L.; Michaelsson, E.; Rosenkranz, S.; Rudolph, T. K.; Hazen, S. L.; Klose, H.; Schermuly, R. T.; Rudolph, V.; Baldus, S. Myeloperoxidase aggravates pulmonary arterial hypertension by activation of vascular Rho-kinase. *JCI Insight* **2018**, *3* (11), 1−17, DOI: 10.1172/jci.insight.97530.
(33) Antonelou, M.; Michaelsson, E.; Evans, R. D.R.; Wang, C. J.; Henderson, S. R.; Walker, L. S.K.; Unwin, R. J.; Salama, A. D. Therapeutic myeloperoxidase inhibition attenuates neutrophil activation, ANCA-mediated endothelial damage, and crescentic GN. *J. Am. Soc. Nephrol* **2020**, *31* (2), 350−364.
(34) Koop, A. C.; Thiele, N. D.; Steins, D.; Michaelsson, E.; Wehmeyer, M.; Scheja, L.; Steglich, B.; Huber, S.; Schulze Zur Wiesch, J.; Lohse, A. W.; Heeren, J.; Kluwe, J. Therapeutic targeting of myeloperoxidase attenuates NASH in mice. *Hepatol Commun.* **2020**, *4* (10), 1441−1458.
(35) Baldus, S.; Rudolph, V.; Roiss, M.; Ito, W. D.; Rudolph, T. K.; Eiserich, J. P.; Sydow, K.; Lau, D.; Szocs, K.; Klinke, A.; Kubala, L.; Berglund, L.; Schrepfer, S.; Deuse, T.; Haddad, M.; Risius, T.; Klemm, H.; Reichenspurner, H. C.; Meinertz, T.; Heitzer, T. Heparins increase endothelial nitric oxide bioavailability by liberating vessel-immobilized myeloperoxidase. *Circulation* **2006**, *113* (15), 1871−1878.
(36) Matsuzawa, Y.; Kwon, T. G.; Lennon, R. J.; Lerman, L. O.; Lerman, A. Prognostic value of flow-mediated vasodilation in brachial artery and fingertip artery for cardiovascular events: a systematic review and meta-analysis. *J. Am. Heart Assoc* **2015**, *4* (11), No. e002270, DOI: 10.1161/JAHA.115.002270.
(37) Rudolph, V.; Rudolph, T. K.; Kubala, L.; Clauberg, N.; Maas, R.; Pekarova, M.; Klinke, A.; Lau, D.; Szocs, K.; Meinertz, T.; Boger, R. H.; Baldus, S. A myeloperoxidase promoter polymorphism is independently associated with mortality in patients with impaired left ventricular function. *Free Radic Biol. Med.* **2009**, *47* (11), 1584−1590.
(38) Tang, N.; Wang, Y.; Mei, Q. Myeloperoxidase G-463A polymorphism and susceptibility to coronary artery disease: a meta-analysis. *Gene* **2013**, *523* (2), 152−157.
(39) van Schooten, F. J.; Boots, A. W.; Knaapen, A. M.; Godschalk, R. W.; Maas, L. M.; Borm, P. J.; Drent, M.; Jacobs, J. A. Myeloperoxidase (MPO) −463G->A reduces MPO activity and DNA adduct levels in bronchoalveolar lavages of smokers. *Cancer Epidemiol Biomarkers Prev* **2004**, *13* (5), 828−833.
(40) Mahmood, I.; Balian, J. D. Interspecies scaling: predicting clearance of drugs in humans. Three different approaches. *Xenobiotica* **1996**, *26* (9), 887−895.
(41) Gan, L. M.; Lagerstrom-Fermer, M.; Ericsson, H.; Nelander, K.; Lindstedt, E. L.; Michaelsson, E.; Kjaer, M.; Heijer, M.; Whatling, C.; Fuhr, R. Safety, tolerability, pharmacokinetics and effect on serum uric acid of the myeloperoxidase inhibitor AZD4831 in a randomized, placebo-controlled, phase I study in healthy volunteers. *Br. J. Clin. Pharmacol.* **2019**, *85* (4), 762−770.
(42) Nelander, K.; Lagerstrom-Fermer, M.; Amilon, C.; Michaelsson, E.; Heijer, M.; Kjaer, M.; Russell, M.; Han, D.; Lindstedt, E. L.; Whatling, C.; Gan, L. M.; Ericsson, H. Early clinical experience with AZD4831, a novel myeloperoxidase inhibitor, developed for patients with heart failure with preserved ejection fraction. *Clin Transl Sci.* **2021**, *14* (3), 812−819.
(43) Robak, M. T.; Herbage, M. A.; Ellman, J. A. Synthesis and applications of tert-butanesulfinamide. *Chem. Rev.* **2010**, *110* (6), 3600−3740.
(44) Cogan, D. A.; Liu, G.; Ellman, J. A. Asymmetric synthesis of chiral amines by highly diastereoselective 1,2-additions of organometallic reagents to N-tert-butanesulfinyl imines. *Tetrahedron* **1999**, *55* (29), 8883−8904.
(45) Klaus, S.; Neumann, H.; Zapf, A.; Strubing, D.; Hubner, S.; Almena, J.; Riermeier, T.; Gross, P.; Sarich, M.; Krahnert, W. R.; Rossen, K.; Beller, M. A general and efficient method for the formylation of aryl and heteroaryl bromides. *Angew. Chem., Int. Ed. Engl.* **2006**, *45* (1), 154−158.

https://doi.org/10.1021/acs.jmedchem.1c02141
J. Med. Chem. 2022, 65, 11485−11496